COMMUNICATIONS CHEMISTRY

ARTICLE

https://doi.org/10.1038/s42004-019-0165-9 OPEN

Photomagnetic effects in metal-free liquid crystals

Takuya Akita[1], Yuki Sugiyama[1], Taira Yamazaki[1], Sho Nakagami[1], Daichi Kiyohara[1], Yoshiaki Uchida[1] & Norikazu Nishiyama[1]

Metal-free liquid-crystalline (LC) materials consisting of a LC nitroxide radical compound exhibit light-induced reversible switching of the magnetic properties as a new photomagnetic effect. This behavior is based on the abrupt change of magnetic properties at the phase transition directly from a chiral smectic C phase to an isotropic liquid (Iso) phase. The origin of the abrupt change is probably the difference in the inhomogeneity of the intermolecular magnetic interactions between LC and Iso phases. To our knowledge, there are no existing reports on a material showing the reversible and quick phase transitions with the large difference of the inhomogeneity. Here we show a relatively simple way to design a compound to enlarge the difference between LC and Iso phases and to make the response quick and reversible. In addition, the presented analysis method that mines Gaussian components from electron paramagnetic resonance spectra enables us to precisely evaluate magnetic properties in condensed phases.

[1] Graduate School of Engineering Science, Osaka University, 1-3 Machikaneyama-cho, Toyonaka, Osaka 560-8531, Japan. Correspondence and requests for materials should be addressed to Y.U. (email: yuchida@cheng.es.osaka-u.ac.jp)

Liquid-crystalline (LC) materials show high responsivity to various stimuli due to their collective molecular motion[1]. The high responsivity can lead to developments of LC devices; in fact, LC displays need the control of light propagation by means of the molecular reorientation in applied electric fields[2]. Conversely, the properties of LC materials can strongly respond to light stimuli; e.g., azobenzene-based or doped LC materials show photo-fluidization[3,4], which induces developments of self-healing abilities of composite gels[5], remote-controllable light shutters[6], light-controllable soft actuators[7,8], and image storages[9,10]. It had been natural that magnetic properties of metal-free compounds are undetectably weak in high-temperature LC phases unlike the above-mentioned properties until some metal-free LC compounds with a stable nitroxide radical moiety in the mesogen core or as one of the terminal groups (LC-NRs) were reported to exhibit the detectable change in magnetic properties at their melting points (Fig. 1a)[11–19].

Despite the radical moiety, LC-NRs are thermally stable up to about 150 °C in the air and in water, and a lot of analogs showing a variety of LC phases have been reported[11,14,15,17,20–26]. Moreover, spin glass-like inhomogeneous magnetic interactions occur in fluid (Fl) phases: LC and isotropic (Iso) phases[13]. The difference in the inhomogeneity of the interactions is likely to result in that in the magnetic properties. Since crystalline (Cr) phases have uniform intermolecular interactions, whereas Fl phases have the most inhomogeneous ones[13,14], the abrupt large changes of magnetic properties occur only at Cr-to-Fl phase transitions thus far[13–15,17,18]. However, such transitions from or to Cr phases are usually irreversible and/or too slow. In contrast, since LC-to-Iso phase transitions, which are transitions between Fl phases, are reversible and fast, these can immediately occur in response to external stimuli like not only temperature but also light. Thus, LC materials consisting of the magnetic LC compounds could exhibit light-induced reversible switching of magnetic properties as a new photomagnetic effect (Fig. 1b). However, since the magnetic properties of the previously reported LC-NRs hardly change at the LC-to-Iso phase transitions[12–19], we have to design a new compound showing the large change of magnetic properties at the LC-to-Iso phase transitions to realize the light-induced reversible switching.

Organic chemists can concisely design molecules in the order of atoms specially for the target stimulus to which LC materials responds; the simplest way to design such a compound is to enlarge the difference in the inhomogeneity of the intermolecular magnetic interactions between LC and Iso phases in terms not only of orientational order[14] but also of one- or two-dimensional (1-D or 2-D) positional order. We focused on rod-like mesogens with more than three side chains, so-called forked structure; the nanophase separation of flexible aliphatic chains from rigid aromatic units results in a high layer order in their LC phases[27]. Accordingly, an LC-NR with the forked structure could show high orientational and layer, that is 1-D positional, orders in LC phases that should induce the large abrupt change of magnetic properties at the LC-to-Iso phase transition.

Here, we report the synthesis of the first example of LC-NRs to the best of our knowledge, with the forked structure as shown in Fig. 1a. The changes of magnetic properties at the temperature-induced phase transitions in the forked LC-NRs (2*S*,5*S*)-**8NO8$_2$** and (±)-**8NO8$_2$** are evaluated by means of superconducting quantum interference device (SQUID) magnetometry and variable-temperature electron paramagnetic resonance (VT-EPR) spectroscopy. We demonstrate the photomagnetic effect of metal-free LC materials consisting of (2*S*,5*S*)-**8NO8$_2$** and an azobenzene analog. In addition, in the course of the analysis of the VT-EPR spectra, a more detailed analysis method for magnetic properties unique to LC phases has been developed to discuss the temperature dependence of paramagnetic susceptibility with high accuracy and the influence of the inhomogeneous intermolecular contacts in detail.

Results

Phase transition. Compounds (2*S*,5*S*)-**8NO8$_2$** and (±)-**8NO8$_2$** were prepared by the synthetic procedure shown in Supplementary Fig. 1 and characterized by high performance liquid chromatography (HPLC) analysis, infrared (IR) spectroscopy, nuclear magnetic resonance (NMR) spectroscopy, and high resolution mass spectrometry (HRMS) (Supplementary Figs. 2–5). The phase transition temperatures of (2*S*,5*S*)-**8NO8$_2$** and (±)-**8NO8$_2$** were determined by differential scanning calorimetry (DSC) at a scanning rate of 2 °C/min upon first heating and cooling processes as shown in Supplementary Fig. 6, variable temperature X-ray diffraction (VT-XRD) analyses in the first heating process as shown in Supplementary Figs. 7 and 8, and polarized optical microscopy (POM) as shown in Supplementary Fig. 9; (2*S*,5*S*)-**8NO8$_2$** shows an enantiotropic chiral smectic C (SmC*) phase between 44.3 °C and 53.8 °C, and (±)-**8NO8$_2$** shows a monotropic smectic C (SmC) phase (see Supplementary Discussion). The chiral nematic (N*) and nematic (N) phases for (2*S*,5*S*)-**8NO8** and (±)-**8NO8** are replaced with SmC* and SmC phases for (2*S*,5*S*)-**8NO8$_2$** and (±)-**8NO8$_2$**, respectively[11], owing to the additional octyloxy side chain. The nanophase separation between incompatible parts of the forked mesogens, abundant

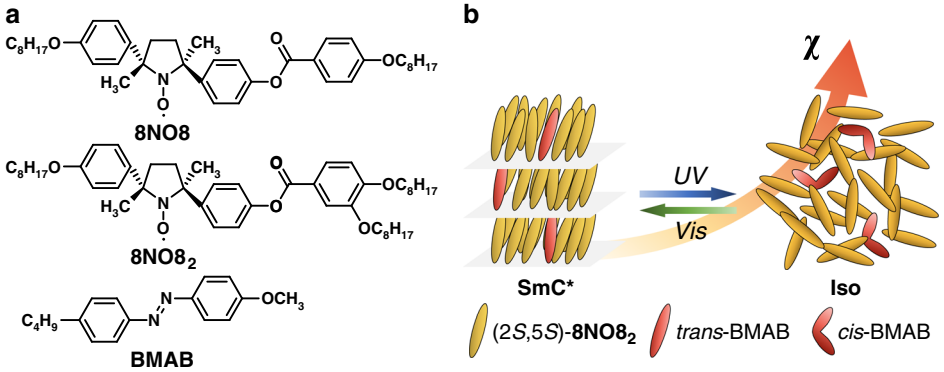

Fig. 1 Molecules and properties of the present LC mixture. **a** Molecular structures of (2*S*,5*S*) enantiomers of compounds **8NO8**, **8NO8$_2$**, and **BMAB**. **b** Photomagnetic effect in a metal-free LC system consisting of (2*S*,5*S*)-**8NO8$_2$** and an azobenzene analog, BMAB. SmC* denotes chiral smectic C, and Iso denotes isotropic liquid. Ultraviolet (UV) and visible (Vis) lights induce *trans*-to-*cis* and *cis*-to-*trans* photoisomerization of BMAB, respectively. When SmC* material dissolving BMAB is irradiated with UV light, *cis*-BMAB disturbs the SmC* structure, and therefore, SmC*-to-Iso phase transition can occur. When the SmC* material consists mainly of nitroxide radicals, the magnetic susceptibility (χ) can increase at the photo-induced SmC*-to-Iso phase transition

Table 1 Thermal properties of LC materials

Compound	*ee* [%][a]	Phase transition [°C][b]	ΔH [kJ mol^{-1}][b]	ΔS [J K^{-1} mol^{-1}][b]
(2*S*,5*S*)-**8NO8**[c]	95.8	Cr 71.2N* 97.6 Iso	2.17	5.85
(±)-**8NO8**[c]	0	Cr 71.5N 103.1 Iso	2.22	5.90
(2*S*,5*S*)-**8NO8$_2$**	>99	Cr 44.3 SmC* 53.8 Iso	9.00	27.5
(±)-**8NO8$_2$**	0	Cr 76.1 (SmC 54.1) Iso	9.64	29.5
(2*S*,5*S*)-**8NO8$_2$** + BMAB[d]	>99	SmC* 51.2 Iso	8.66	26.7

[a]Determined by HPLC analyses on a chiral stationary phase column
[b]Determined by DSC analyses upon the first heating or cooling processes
[c]The data were reported in ref. [11]
[d]The concentration of BMAB is 5.1 mol%

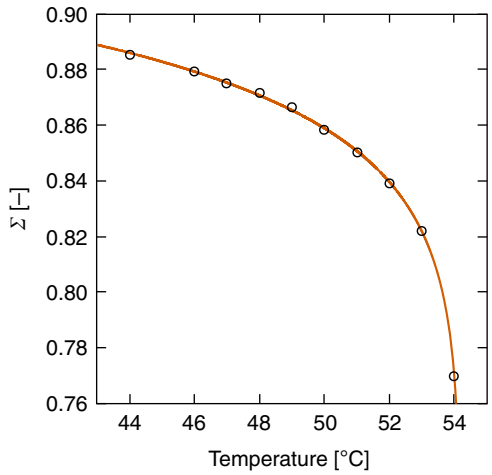

Fig. 2 Temperature dependence of translational order parameter Σ in the SmC* phase of (2*S*,5*S*)-**8NO8$_2$**. In the cooling process, Σ reaches quite high values up to 0.9. In addition, note that Σ starts to increase sharply from a little above the Iso-to-SmC* phase transition. Open circles represent the experimental data and solid line denotes the fitting curve

flexible aliphatic chains and rigid aromatic units, is likely to induce layer order and biaxiality[27].

In addition, it is worth noting that **8NO8$_2$** have larger transition enthalpy ΔH (~4.5 times) and transition entropy ΔS (~5 times) at the clearing points than **8NO8** as summarized in Table 1. The increase of ΔH indicates that the forked mesogens **8NO8$_2$** have larger intermolecular interactions which induce both higher orientational and layer ordering in the SmC* and SmC phases. Furthermore, the increase of ΔS indicates that **8NO8$_2$** has the fewer number of possible conformations and configurations in the SmC* and SmC phases than **8NO8** in N* and N phases if the conformations and configurations are equally random in both the Iso phases of **8NO8** and **8NO8$_2$**. Therefore, it is easy to anticipate that the inhomogeneity of the intermolecular contacts sharply increases at the LC-to-Iso phase transition of **8NO8$_2$**; the large abrupt change of paramagnetic susceptibility could occur at the phase transition.

Detailed insight into SmC* structure. VT-XRD measurements allow the calculation of the translational order parameter Σ, so-called smectic order parameter, providing information of the quality of the translational periodicity of the smectic layers, and the correlation length ξ for the smectic ordering (Supplementary Discussion and Supplementary Figs. 10 and 11). The temperature dependence of Σ in the SmC* phase of (2*S*,5*S*)-**8NO8$_2$** can be estimated from the integrated temperature-dependent scattering intensity $A_{XRD}(T)$ of the peak for (001) according to previously developed method (see Supplementary Methods)[28]. The experimental $A_{XRD}(T)$ data are well reproduced by Eq. (1) as shown in Supplementary Fig. 10 with the values of $T_C = 3.2733(3) \times 10^2$ K, $A_{XRD}{}^0 = 1.88(1) \times 10^4$, and $\beta = 3.48(7) \times 10^{-2}$, which are comparable with the previously reported experimental values for SmC* materials[28].

$$A_{XRD}(T) = A^0_{XRD}\left[1 - \frac{T}{T_C}\right]^{2\beta} \quad (1)$$

The obtained Σ value for (2*S*,5*S*)-**8NO8$_2$** is larger than that for conventional thermotropic LC compounds, which usually ranges around 0.7, as shown in Fig. 2[28,29]. It implies that the molecules are rarely dislocated out of the smectic layers. The specificity in Σ value of (2*S*,5*S*)-**8NO8$_2$** perhaps reflects both steric aggregability of side chains arising from intercalation to reduce free volume and electrostatic aggregation of rigid cores originating from large lateral dipole on the nitroxide. It reminds us that the similar situation of compounds showing high Σ value around 0.9 possesses specific side groups such as siloxane[30–32], fluorinated carbon groups[32], polar groups[32], and ionic moiety[33,34], which strongly repel rigid core and/or attract adjacent side chains.

Magnetic properties. To compare the magnetic properties in the Cr, LC, and Iso phases, first, we have to confirm the magnetic interactions in the Cr phases because the magnetic properties in Cr phase serve as references for those in Fl phases. Molar magnetic susceptibility χ_M for (2*S*,5*S*)-**8NO8$_2$** and (±)-**8NO8$_2$** is available by means of SQUID magnetometry in a magnetic field of 0.5 T in the temperature range of 2–300 K in the first heating process. The obtained results indicate that the NO groups are chemically stable and that the crystals of (2*S*,5*S*)-**8NO8$_2$** and (±)-**8NO8$_2$** show weak intermolecular antiferromagnetic interactions at low temperature ($\theta < 0$ and $J < 0$, Supplementary Fig. 12, Supplementary Table 1 and Supplementary Discussion).

In turn, we measured the temperature dependence of paramagnetic susceptibility χ_{para} of (2*S*,5*S*)-**8NO8$_2$** between 313 and 340 K (40 and 67 °C) by means of SQUID magnetometry in a magnetic field of 0.05 T (Fig. 3). The χ_{para}–T and $\chi_{para}T$–T plots seem to obey the Curie–Weiss law in the temperature range between 313 and 327 K, where Curie constant $C = 0.398$ emu K mol^{-1} and Weiss constant $\theta = -0.032$ K, respectively. The χ_{para} value seems mostly unchanged at the Cr-to-SmC* phase transition. In contrast, the experimental χ_{para} of (2*S*,5*S*)-**8NO8$_2$** in the Iso phase is larger than that estimated from the Curie and Weiss constants for the lower-temperature phases; χ_{para} and $\chi_{para}T$ increase at the SmC*-to-Iso phase transition (1.7% at 330 K in 0.05 T) as shown in Fig. 3, which is referred to as the positive magneto-LC effect[15]. As expected, the change ratios of the χ_{para} values at the Cr-to-LC and LC-to-Iso phase transitions for (2*S*,5*S*)-**8NO8$_2$** are unusual; previously reported LC-NRs show larger change ratios at Cr-to-LC phase transitions than those at LC-to-Iso phase transitions.

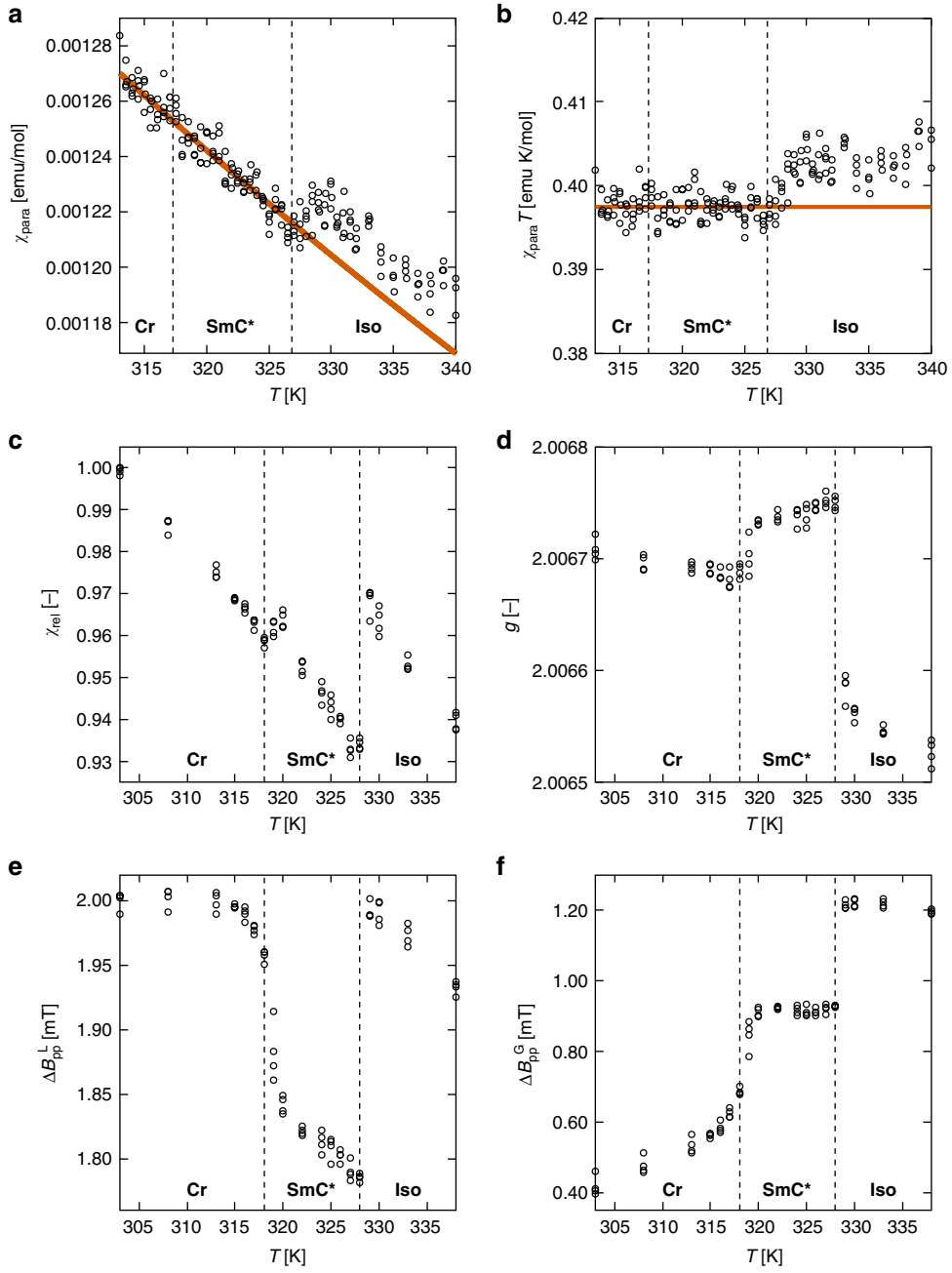

Fig. 3 Temperature-dependent magnetic properties for (2*S*,5*S*)-**8NO8$_2$**. **a** χ_{para}–*T* plot and **b** $\chi_{para}T$–*T* plot in a magnetic field of 0.05 T. The circles denote the experimental data in the first heating process, the solid lines denote the Curie–Weiss curve with $C = 0.398$ emu K mol^{-1} and $\theta = -0.032$ K fitted between 313 and 327 K. Temperature dependence of **c** χ_{rel}, **d** *g*-value, **e** $\Delta B_{pp}{}^{L}$, and **f** $\Delta B_{pp}{}^{G}$ for (2*S*,5*S*)-**8NO8$_2$** obtained by EPR spectroscopy in a magnetic field of 0.33 T in the first heating process. Vertical dashed lines denote the Cr-to-SmC* and SmC*-to-Iso phase transition temperatures determined from the peaks in the DSC charts and *g*-value changes

A clue to the origin of these new phenomena should come from a close examination of the difference in intermolecular interactions between the phases by means of EPR spectroscopy (Supplementary Fig. 13), which also gives the temperature dependence of χ_{para}[13,14]. To improve the accuracy to estimate the temperature dependence of χ_{para}, we have developed the following method; the experimental EPR spectra are fitted with the area-normalized pseudo-Voigtian derivative instead of Lorentzian derivative used in the previously reported method (see Supplementary Figs. 14 and 15)[13]. The new method excels in the deconvolution of experimental EPR spectra and can include Gaussian contributions in χ_{para} values with high accuracy (see Supplementary Discussion)[14]. The temperature dependence of relative paramagnetic susceptibility χ_{rel} for (2*S*,5*S*)-**8NO8$_2$** showed a small χ_{rel} increase by 0.55% at the Cr-to-SmC* phase transition (from 45 to 47 °C) as shown in Fig. 3c. Moreover, it is noteworthy that χ_{rel} increased by 3.7% at the SmC*-to-Iso phase transition (from 55 to 56 °C), which is larger than that at the Cr-to-SmC* phase transition. These phenomena are consistent with those from SQUID magnetometry (Fig. 3a). Among all NR compounds, (2*S*,5*S*)-**8NO8$_2$** shows the largest increase of χ_{para} at the LC-to-Iso phase transition. For the LC-NRs, the anisotropy of paramagnetic susceptibility $\Delta\chi_{para}$, which is theoretically proportional to the anisotropy of g^2, does not seem to cause the changes

of χ_{rel} as shown in Fig. 3d (see Supplementary Discussion). This unfamiliar trend is likely to be attributed to the LC nature of (2*S*,5*S*)-**8NO8$_2$**, which is similar to the Cr phase rather than the Iso phase. In addition, (±)-**8NO8$_2$** also shows the similar phenomena at the phase transition to the Iso phase in the heating process (Supplementary Fig. 16).

Next, the correlation between the temperature dependence of χ_{rel} and that of the parameters estimated from EPR spectra should give an interpretation of the phenomena (Fig. 3). The deconvolution of the Voigtian EPR spectra gives two types of temperature-dependent peak-to-peak linewidths, Lorentzian linewidth $\Delta B_{pp}{}^{L}$ and Gaussian linewidth $\Delta B_{pp}{}^{G}$ as shown in Fig. 3. Generally, $\Delta B_{pp}{}^{L}$ reflects the following two magnetic interactions: (a) spin–spin dipolar interactions (the stronger the interaction is, the more the $\Delta B_{pp}{}^{L}$ increases) and (b) spin–spin exchange interactions (the stronger the interaction is, the more the $\Delta B_{pp}{}^{L}$ decreases)[13,15]. Meanwhile, $\Delta B_{pp}{}^{G}$ reflects the inhomogeneous broadening of the EPR spectra, which is useful to discuss the contribution of the inhomogeneity of the intermolecular magnetic interactions to the magneto-LC effects[14].

The temperature dependence of $\Delta B_{pp}{}^{L}$ around the SmC*-to-Iso phase transition is different from that around the Cr-to-SmC* phase transition; the abrupt large increase in $\Delta B_{pp}{}^{L}$ occurred in concert with the abrupt increase in χ_{rel} at the SmC*-to-Iso phase transition in the heating process (Fig. 3), indicating the generation of ferromagnetic spin–spin dipolar interactions in the Iso phase and/or the extinction of antiferromagnetic spin–spin exchange interactions. The delicate balance of the two factors is likely to give rise to the complicated behavior of temperature dependence of $\Delta B_{pp}{}^{L}$. However, we could say that $\Delta B_{pp}{}^{G}$ is the dominant factor for the χ_{rel} change (Fig. 3). The large increase of $\Delta B_{pp}{}^{G}$ at the SmC*-to-Iso phase transition indicates that the additional appearance of inhomogeneity of intermolecular magnetic interactions in the Iso phase. These results suggest that the intermolecular magnetic interactions can become more inhomogeneous even at the SmC*-to-Iso phase transition, and the averaged ferromagnetic interactions further increase in the Iso phase.

To gain an insight into the origin of the changes of χ_{rel}, $\Delta B_{pp}{}^{L}$, and $\Delta B_{pp}{}^{G}$ at SmC*-to-Iso phase transition, we have to focus on the structural details of intermolecular contacts in these Fl phases. The estimated correlation length ξ for the smectic ordering (Supplementary Fig. 12) indicates that molecules contact with each other in the same manner in the range up to about 80 nm in length. Based on the tendency that the intermolecular magnetic interactions between nearest molecules dominate magnetic properties of organic radicals with localized spins[35], it can be considered that the 80 nm is much longer in terms of intermolecular magnetic interactions. Thus, the intermolecular magnetic interactions are considered to be sufficiently homogeneous in the SmC* phase of (2*S*,5*S*)-**8NO8$_2$**. In addition, the high smectic order parameter Σ of (2*S*,5*S*)-**8NO8$_2$** even in the vicinity of Iso-to-SmC* phase transition (Fig. 2) implies that the molecules in the SmC* phase are little dislocated out of the layers and are arranged in Cr-like manner. And this high Σ is consistent with large transition entropy ΔS at SmC*-to-Iso phase transition (Table 1). These results mean that the intermolecular magnetic interactions in the SmC* phase of (2*S*,5*S*)-**8NO8$_2$** are similar to those in the Cr phase over the whole system. Thus, the loss of the Cr-like layer order in the SmC* phase should induce the large increase of inhomogeneity of the intermolecular contacts and of averaged intermolecular ferromagnetic interactions, leading to the large abrupt change of χ_{rel}, at the SmC*-to-Iso phase transition. Therefore, as a guideline to prepare LC-NRs showing large increases of χ_{para} at LC-to-Iso phase transitions, additional aliphatic side chain is likely to be effective because it induces not only orientational order but also high layer order in the LC phases.

Reversible switching of magnetic properties. With the effective use of this large change of magnetic properties at SmC*-to-Iso phase transition, temperature change could induce the reversible switching of magnetic properties. The parameters estimated from EPR spectra for (2*S*,5*S*)-**8NO8$_2$** at $T_{CP} - 2 = 52$ °C and $T_{CP} + 2 = 56$ °C, where T_{CP} is a clearing point, are different from each other; e.g., χ_{rel} increases by 4.5% as temperature increases from 52 to 56 °C, and it returns to the initial value as temperature returns (Fig. 4a). In contrast to conventional solid-state magnetic materials showing a decrease of magnetic susceptibility with increasing temperature, it is noteworthy that (2*S*,5*S*)-**8NO8$_2$** exhibits an increase of magnetic susceptibility with increasing temperature. Besides, the absolute value of the variation of χ_{rel} for (2*S*,5*S*)-**8NO8$_2$** (4.5%) is much larger than that expected from Curie law for usual paramagnetic materials (1.2%) (see Supplementary Discussion). Furthermore, all the parameters of (2*S*,5*S*)-**8NO8$_2$** also show reversible switching (Fig. 4b–d). These results indicate that the changes of inhomogeneity of intermolecular magnetic interactions through the temperature-change-induced phase transitions contribute to the magnetic switching as mentioned above and that (2*S*,5*S*)-**8NO8$_2$** is stable against repeated heating and cooling processes.

We focused on light irradiation as one of the other external stimuli to induce the SmC*-to-Iso and Iso-to-SmC* phase transitions because light stimuli can be controlled much more quickly than temperature. According to previous reports[3,9], for the photo-induced switching of the magnetic properties, we doped 4-butyl-4′-methoxyazobenzene (BMAB) into (2*S*,5*S*)-**8NO8$_2$** by 5.1 mol% (Fig. 5 and Supplementary Fig. 17). It induces photo-fluidization originating from photoisomerization of the azobenzene moiety; the UV and visible lights cause its *trans*-to-*cis* and *cis*-to-*trans* photoisomerization, respectively (see Supplementary Methods)[3,9]. The phase transition of the photo-responsive magnetic LC mixture was characterized by POM (Supplementary Fig. 18) and DSC (Supplementary Fig. 19) analyses (see Supplementary Discussion). The mixture shows an enantiotropic SmC* phase from room temperature to 51.2 °C in the DSC chart; the doped BMAB does not extinguish the intrinsic LC nature of (2*S*,5*S*)-**8NO8$_2$**. Actually, we confirmed that the UV light (365 nm) and visible light (530 nm) repeatedly induce SmC*-to-Iso and Iso-to-SmC* phase transitions at 52.4 °C in the POM, respectively. To find the most appropriate temperature for the photo-induced magnetic switching, we measured the temperature dependence of paramagnetic susceptibility of the photo-responsive magnetic LC mixture in dark or under UV light irradiation by means of EPR spectroscopy. The χ_{rel} abruptly increased at 52 °C in dark, whereas it gradually increased around 45 °C under UV light irradiation (Fig. 5). The variation of the transition temperature should be attributed to the variation of the concentration of *cis* isomer of BMAB. The most appropriate temperature is likely to be 51 °C.

We examined if the photo-induced magnetic switching occurs in the LC mixture at 51 °C as shown in Fig. 5 (Supplementary Fig. 20). All magnetic properties reversibly change under the UV and visible light irradiation; the behavior resembles the temperature-change-induced switching (Fig. 4). These results also indicate that both (2*S*,5*S*)-**8NO8$_2$** and BMAB are stable under the UV irradiation. We can conclude that the photo-induced SmC*-to-Iso and Iso-to-SmC* phase transitions causes the magnetic switching as shown in Fig. 1b; in fact, the changes of magnetic properties were too small to be recognized at 60 °C, where Iso phase is the most stable even under visible light

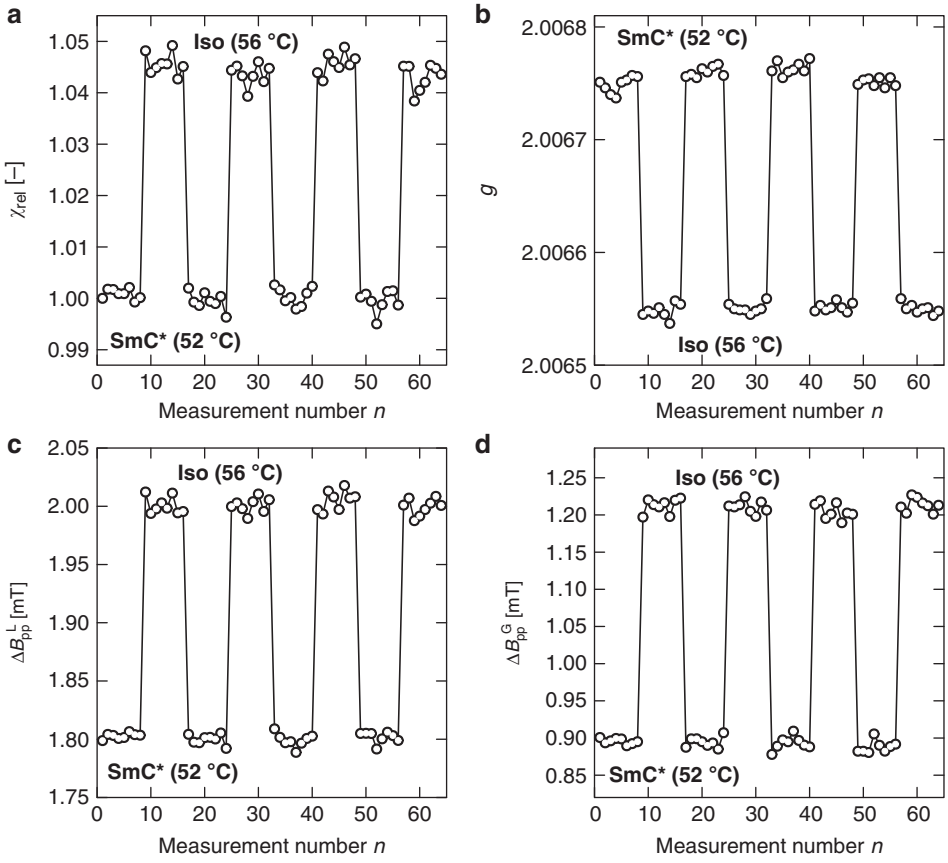

Fig. 4 Switching of the magnetic properties of (2*S*,5*S*)-**8NO8$_2$**. Switching of **a** χ_{rel}, **b** *g*-value, **c** $\Delta B_{pp}{}^{L}$, and **d** $\Delta B_{pp}{}^{G}$ was measured by EPR spectroscopy in a magnetic field of 0.33 T at 52 or 56 °C

irradiation. This is the first example of photomagnetic effects in condensed fluid phases of organic radicals above room temperature.

Discussion

We have successfully prepared a magnetic soft material showing light-responsive magnetic properties, which consists mainly of a chiral nitroxide radical (2*S*,5*S*)-**8NO8$_2$** showing a highly ordered SmC* phase. Its forked mesogen is likely to induce strong magneto-LC effects at the SmC*-to-Iso phase transition. The switching of magnetic properties is reversible and stable against repeated irradiation of light as well as temperature change. Besides, in principle, the switching by applying electric fields would be also possible if the SmC* phase shows ordered polarization states like ferroelectric or antiferroelectric state when it is introduced into a thin cell[16]. In general, the induction of highly ordered LC phases is crucial to this system. The large responsivity due to the collective molecular motion in LC phases, which is not available in solid phases, results in these unique magnetic properties switchable by various external stimuli. The design of magnetic soft materials, which utilizes the large abrupt change of magnetic properties at LC-to-Iso phase transition, has potential to open new routes to materials with potentially useful applications. In addition, the discussed analysis method, which mines Gaussian components from EPR spectra, enables us to evaluate magnetic properties in fluid phases.

Methods

Synthetic procedures. See Supplementary Methods and Supplementary Fig. 1.

Characterization of LC-NRs. See Supplementary Methods and Supplementary Figs. 2–5.

Phase transition of LC-NRs. See Supplementary Methods and Supplementary Figs. 6–9.

Translational order parameters in the SmC* phase. See Supplementary Methods and Supplementary Fig. 10.

Tilt angles in the SmC* phase. See Supplementary Methods.

Correlation lengths in the SmC* phase. See Supplementary Methods and Supplementary Fig. 11.

Evaluation of magnetic properties from SQUID magnetometry. See Supplementary Methods, Supplementary Fig. 12, and Supplementary Table 1.

Derivation of magnetic properties from EPR spectroscopy. See Supplementary Methods and Supplementary Figs. 13–16.

Preparation of photo-responsive magnetic LC mixture. See Supplementary Methods and Supplementary Fig. 17.

Phase transition of photo-responsive magnetic LC mixture. See Supplementary Methods and Supplementary Figs. 18 and 19.

Photo-responsive magnetic properties. See Supplementary Methods and Supplementary Fig. 20.

Data and code availability

All data generated during the current study are available in this article and the Supplementary Information file or from the corresponding author on reasonable request.

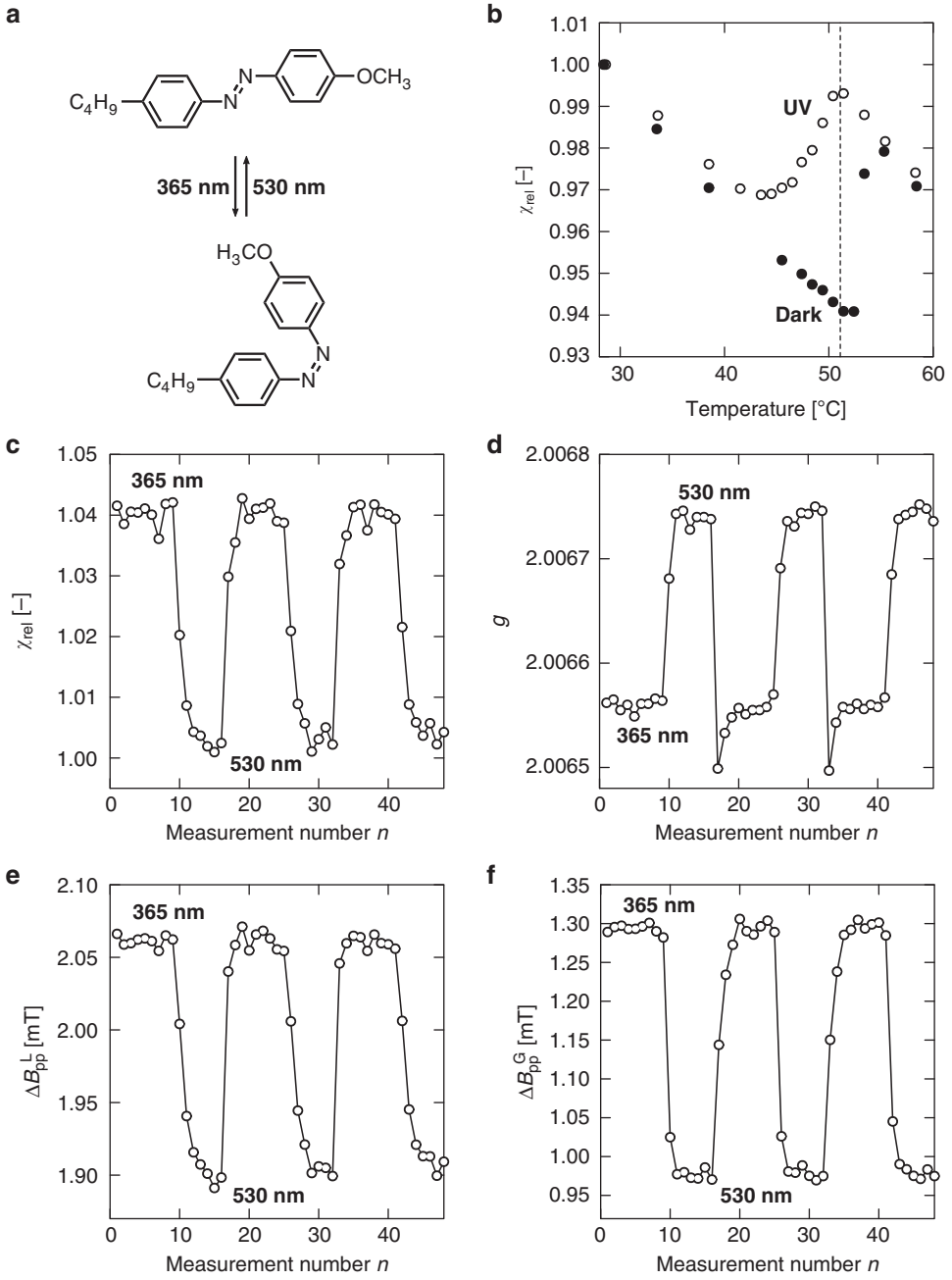

Fig. 5 Photomagnetic effects in LC mixture of (2*S*,5*S*)-**8NO8$_2$** and BMAB. **a** Molecular structure and photoisomerization of BMAB. **b** Temperature dependence of χ_{rel} for photo-responsive magnetic LC mixture of (2*S*,5*S*)-**8NO8$_2$** and BMAB by EPR spectroscopy in a magnetic field of around 0.33 T in the heating processes in dark (closed circles) and under UV light irradiation (open circles). Error bars are not shown because they are sufficiently small. Vertical dashed line denotes the clearing point under UV light irradiation expected by DSC analysis. Switching of **c** χ_{rel}, **d** *g*-value, **e** $\Delta B_{pp}{}^{L}$, and **f** $\Delta B_{pp}{}^{G}$ for photo-responsive magnetic LC mixture was measured by EPR spectroscopy in a magnetic field of 0.33 T. The data were obtained from EPR spectra measured under UV and visible light irradiation at 51 °C

Received: 26 November 2018 Accepted: 17 May 2019
Published online: 07 June 2019

References

1. Collings, P. J. & Hird, M. *Introduction to Liquid Crystals: Chemistry and Physics*. (CRC Press, Boca Raton, FL, 1997).
2. Kirsch, P. & Bremer, M. Nematic liquid crystals for active matrix displays: molecular design and synthesis. *Angew. Chem. Int. Ed.* **39**, 4216–4235 (2000).
3. Tazuke, S., Kurihara, S. & Ikeda, T. Amplified image recording in liquid crystal media by means of photochemically triggered phase transition. *Chem. Lett.* **16**, 911–914 (1987).
4. Ikeda, T. Photomodulation of liquid crystal orientations for photonic applications. *J. Mater. Chem.* **13**, 2037–2057 (2003).
5. Kawata, Y., Yamamoto, T., Kihara, H. & Ohno, K. Dual self-healing abilities of composite gels consisting of polymer-brush-afforded particles and an azobenzene-doped liquid crystal. *ACS Appl. Mater. Interfaces* **7**, 4185–4191 (2015).
6. Kim, D.-Y. et al. An azobenzene-based photochromic liquid crystalline amphiphile for a remote-controllable light shutter. *Chem. Commun.* **51**, 11080–11083 (2015).

7. Harris, K. D. et al. Large amplitude light-induced motion in high elastic modulus polymer actuators. *J. Mater. Chem.* **15**, 5043–5048 (2005).
8. Yu, Y. & Ikeda, T. Soft actuators based on liquid-crystalline elastomers. *Angew. Chem. Int. Ed.* **45**, 5416–5418 (2006).
9. Ikeda, T. & Tsutsumi, O. Optical switching and image storage by means of azobenzene liquid-crystal films. *Science* **268**, 1873–1875 (1995).
10. Shishido, A. Rewritable holograms based on azobenzene-containing liquid-crystalline polymers. *Polym. J* **42**, 525–533 (2010).
11. Ikuma, N. et al. Magnetic properties of all-organic liquid crystals containing a chiral five-membered cyclic nitroxide unit within the rigid core. *Angew. Chem. Int. Ed.* **43**, 3677–3682 (2004).
12. Uchida, Y. et al. Magnetic-field-induced molecular alignment in an achiral liquid crystal spin-labeled by a nitroxyl group in the mesogen core. *J. Mater. Chem.* **19**, 415–418 (2008).
13. Uchida, Y. et al. Anisotropic and inhomogeneous magnetic interactions observed in all-organic nitroxide radical liquid crystals. *J. Am. Chem. Soc.* **132**, 9746–9752 (2010).
14. Uchida, Y., Suzuki, K. & Tamura, R. Magneto-LC effects in hydrogen-bonded all-organic radical liquid crystal. *J. Phys. Chem. B* **116**, 9791–9795 (2012).
15. Suzuki, K., Uchida, Y., Tamura, R., Shimono, S. & Yamauchi, J. Observation of positive and negative magneto-LC effects in all-organic nitroxide radical liquid crystals by EPR spectroscopy. *J. Mater. Chem.* **22**, 6799–6806 (2012).
16. Suzuki, K. et al. Influence of applied electric fields on the positive magneto-LC effects observed in the ferroelectric liquid crystalline phase of a chiral nitroxide radical compound. *Soft Matter* **9**, 4687–4692 (2013).
17. Suzuki, K. et al. Chiral all-organic nitroxide biradical liquid crystals showing remarkably large positive magneto-LC effects. *Chem. Commun.* **52**, 3935–3938 (2016).
18. Akita, T., Yamazaki, T., Uchida, Y. & Nishiyama, N. Magnetic properties of terminal iodinated nitroxide radical liquid crystals. *Polyhedron* **136**, 79–86 (2017).
19. Bajzíková, K. et al. All-organic liquid crystalline radicals with a spin unit in the outer position of a bent-core system. *J. Mater. Chem. C* **4**, 11540–11547 (2016).
20. Tamura, R., Uchida, Y. & Ikuma, N. Paramagnetic all-organic chiral liquid crystals. *J. Mater. Chem.* **18**, 2872–2876 (2008).
21. Ikuma, N. et al. Ferroelectric properties of paramagnetic, all-organic, chiral nitroxyl radical liquid crystals. *Adv. Mater.* **18**, 477–480 (2006).
22. Uchida, Y. et al. Synthesis and characterization of novel all-organic liquid crystalline radicals. *Mol. Cryst. Liq. Cryst.* **479**, 213–221 (2007).
23. Uchida, Y., Suzuki, K., Tamura, R., Aoki, Y. & Nohira, H. Pretransitional layer contraction at the chiral smectic a-to-chiral smectic C phase transition of a chiral nitroxide radical. *J. Phys. Chem. B* **117**, 3054–3060 (2013).
24. Akita, T., Uchida, Y. & Nishiyama, N. Terminal fluorinated nitroxide radical liquid crystalline compounds. *Mol. Cryst. Liq. Cryst.* **613**, 174–180 (2015).
25. Akita, T., Uchida, Y., Kiyohara, D., Nakagami, S. & Nishiyama, N. Paramagnetic nitroxide radical liquid crystalline compounds with methyl di (ethylene glycol) chain. *Ferroelectrics* **495**, 97–104 (2016).
26. Akita, T., Uchida, Y. & Nishiyama, N. Effects of linking group on liquid crystallinity of nitroxide radical compounds. *Chem. Lett.* **45**, 910–912 (2016).
27. Reddy, R. A. & Tschierske, C. Bent-core liquid crystals: polar order, superstructural chirality and spontaneous desymmetrisation in soft matter systems. *J. Mater. Chem.* **16**, 907–961 (2006).
28. Kapernaum, N. & Giesselmann, F. Simple experimental assessment of smectic translational order parameters. *Phys. Rev. E* **78**, 062701 (2008).
29. Takanishi, Y., Ikeda, A., Takezoe, H. & Fukuda, A. Higher smectic-layer order parameters in liquid crystals determined by x-ray diffraction and the effect of antiferroelectricity. *Phys. Rev. E* **51**, 400–406 (1995).
30. Roberts, J. C. et al. Design of liquid crystals with "de vries-like" properties: frustration between SmA- and SmC-promoting elements. *J. Am. Chem. Soc.* **132**, 364–370 (2010).
31. Prasad, S. K., Rao, D. S. S., Sridevi, S., Naciri, J. & Ratna, B. R. Critical behavior of three organosiloxane de Vries-type liquid crystals observed via the dielectric response. *J. Phys.: Condens. Matter* **23**, 105902 (2011).
32. Gorkunov, M. V., Osipov, M. A., Kapernaum, N., Nonnenmacher, D. & Giesselmann, F. Molecular theory of smectic ordering in liquid crystals with nanoscale segregation of different molecular fragments. *Phys. Rev. E* **84**, 051704 (2011).
33. Wuckert, E. et al. Photoresponsive ionic liquid crystals based on azobenzene guanidinium salts. *Phys. Chem. Chem. Phys.* **17**, 8382–8392 (2015).
34. Kapernaum, N. et al. First examples of de vries-like smectic A to smectic C phase transitions in ionic liquid crystals. *ChemPhysChem* **17**, 4116–4123 (2016).
35. Kinoshita, M. Ferromagnetism of organic radical crystals. *Jpn. J. Appl. Phys.* **33**, 5718–5733 (1994).

Acknowledgements

The authors extend appreciation to Professor Rui Tamura, Kyoto University, for experimental support, including measurement of X-ray diffraction and to Ms. Kaho Yamamoto, Osaka University, for assistance at making fitting programs. This work was supported in part by the Japan Science and Technology Agency (JST) 'Precursory Research for Embryonic Science and Technology (PRESTO)' for a project of 'Molecular technology and creation of new function' and by JSPS KAKENHI Grant Number JP17H04896. T.A. is very grateful to the JSPS Research Fellowships for Young Scientists JP16J05585. The computations were performed using Research Center for Computational Science, Okazaki, Japan.

Author contributions

Y.U. and T.A. designed the study; T.A., Y.S., T.Y., S.N. and D.K. performed the synthesis, the measurements and the analyses of the obtained data; Y.U., T.A. and N.N. wrote the paper. All authors discussed and commented on the paper.

Additional information

Supplementary information accompanies this paper at https://doi.org/10.1038/s42004-019-0165-9.

Competing interests: The authors declare no competing interests.

Reprints and permission information is available online at http://npg.nature.com/reprintsandpermissions/

Publisher's note: Springer Nature remains neutral with regard to jurisdictional claims in published maps and institutional affiliations.